Petroleum Science 20 (2023) 3348–3362

Contents lists available at ScienceDirect

Petroleum Science

journal homepage: www.keaipublishing.com/en/journals/petroleum-science

Original Paper

Hydrocarbon generation differences of shales composed of green algal and cyanobacteria: A case study of Mesozoic and Cenozoic saline lacustrine shales in Junggar Basin, NW China

Miao Yu [a, b], Gang Gao [a, b, *], Wan-Yun Ma [c, d, e], Miao Liu [a, b], Ni Zhou [c, d, e], You-Jin Zhang [a, b], Dan He [c, d, e], Ke-Ting Fan [a, b], Liu-Lin-Bo Guo [a, b], Jie Li [a, b]

[a] College of Geosciences, China University of Petroleum, Beijing, 102249, China
[b] Key Laboratory of Petroleum Resources and Prospecting, China University of Petroleum, Beijing, 102249, China
[c] Research Institute of Experimental Testing, Xinjiang Oilfield Company, PetroChina, Karamay, 834000, Xinjiang, China
[d] Xinjiang Conglomerate Reservoir Laboratory, Karamay, 834000, Xinjiang, China
[e] Key Laboratory of Exploration and Development of Conglomerate Reservoirs, Karamay, 834000, Xinjiang, China

ARTICLE INFO

Article history:
Received 25 October 2022
Received in revised form
26 July 2023
Accepted 20 August 2023
Available online 21 August 2023

Edited by Jie Hao and Teng Zhu

Keywords:
Green algae
Cyanobacteria
Shale
Anjihaihe Formation
Qingshuihe Formation
Junggar Basin

ABSTRACT

The Mesozoic and Cenozoic strata in the Junggar basin developed two sets of shallow to semi-deep lacustrine shale, namely, the Cretaceous Qingshuihe Formation (K_{1q}) and the Paleogene Anjihaihe Formation ($E_{2\text{-}3a}$). Through organic petrology and scanning electron microscope (SEM) observation, it is found that the primary hydrocarbon-generating organic matter (OM) in the two sets of strata is different. The biological precursor of the $E_{2\text{-}3a}$ OM is mainly green algae (*Pediastrum*), while the precursor of K_{1q} kerogen is mainly cyanobacteria (*Oscillatoria*). Then, the $E_{2\text{-}3a}$ green algae-rich shale and K_{1q} cyanobacteria-rich shale were subjected to hydrous pyrolysis and kinetic analysis, respectively. The results show that the evolution modes of hydrocarbon generation of the typical shales are very different. Green algae have the characteristics of a low oil generation threshold, heavy oil quality, and no prominent oil peak, while cyanobacteria have the characteristics of late oil generation, concentrated hydrocarbon generation, and relatively light oil quality. The characteristics of oil generation can also be well reflected in the composition evolution of the crude oil components. The carbon isotope of gas, kerogen, and extracts of the $E_{2\text{-}3a}$ green algae-rich shale are significantly heavier than the K_1q cyanobacteria-rich shale, which may be related to the living habits of their biological precursors, carbon source usage, photosynthesis efficiency, and carbon fixation efficiency.

1. Introduction

As a critical hydrocarbon-generating organic matter (OM) in source rocks, algae have made significant contributions to the formation of oil and gas (Robinson, 1969; Hutton et al., 1980; Collister et al., 2004). Lamalginite is generally considered to be produced by the residue of algae or cyanobacteria, which can be used as a sign of closed environments such as lakes (Collister et al., 2004). Lamalginite in lacustrine sediments mainly comes from cyanobacteria and green algae (Cook and Sherwood, 1991). For example, the kerogen precursors of Alberta shale in Canada (Smith et al., 1991), Upper Paleozoic source rocks in the Timan Pechora Basin in Russia (Collister et al., 2004), Kukersite oil shale in the Baltic Basin in Estonia (Foster et al., 1990), and the Ordovician Marine carbonate source rocks in the Tarim Basin (Pu et al., 1998) are mainly cyanobacteria. The biological precursors of the Rundle type shale in Australia are mainly *Pediastrum* of the green algae family (Hutton et al., 1980; Saxby, 1980; Hutton, 1987), while Green River shale kerogen in the United States is composed of both cyanobacteria and green algae (Robinson, 1969).

Two sets of lacustrine shale are developed in the Mesozoic and Cenozoic in the Junggar basin, including the Cretaceous Qingshuihe Formation (K_{1q}) and the Paleogene Anjihaihe Formation ($E_{2\text{-}3a}$) (Du et al., 2019). Both sets of strata developed Type I-Type II_1 kerogen,

* Corresponding author. College of Geosciences, China University of Petroleum, Beijing, 102249, China.
E-mail address: gaogang2819@sina.com (G. Gao).

https://doi.org/10.1016/j.petsci.2023.08.023

with a high abundance of OM (Wang et al., 2011; Chen et al., 2017). The drilled and outcrop samples are mainly in the immature to low mature stage, while both sets of shales in the depression may have reached the mature stage (Wang et al., 2021). In many regions of the world, well-developed source rocks were found during the Paleogene and Cretaceous sedimentary periods (Klemme and Ulmishek, 1991). With the development of exploration, an increasing number of crude oils related to the $E_{2\text{-}3a}$ and the K_{1q} shales have been found (Chen et al., 2017; Tian et al., 2022; Yu et al., 2022). However, the research on Paleogene and Cretaceous source rocks in the Junggar Basin is still relatively weak, which greatly restricts the related oil and gas exploration work. The purpose of this study is to investigate the main hydrocarbon-generating OM of the $E_{2\text{-}3a}$ and the K_{1q} shales, and then compare their hydrocarbon-generating characteristics. The results of this study are not only of great significance for oil and gas exploration in the Junggar Basin, but also supplement the research on hydrocarbon generation of OM in saline lacustrine source rocks.

2. Regional geology

Junggar Basin, located in northwest Xinjiang Province, China (Fig. 1a), is one of the large superimposed petrol-bearing basins in western China (Chen et al., 2015). The basin is composed of six first-order tectonic units, namely, the western uplift, the eastern uplift, the Luliang uplift, the North Tianshan piedmont thrust belt, the central depression, and the Wulungu Depression (Yang et al., 2004) (Fig. 1b), with multiple sets of strata from the late Paleozoic to the Cenozoic (Wang et al., 2021) (Fig. 1c).

The Ziniquanzi Formation ($E_{1\text{-}2z}$) and the Anjihaihe Formation ($E_{2\text{-}3a}$) developed from the bottom up in the Paleogene in the Junggar Basin, among which, $E_{1\text{-}2z}$ is dominated by oxidized mudstone and siltstone, with no source rock developed. The $E_{2\text{-}3a}$ developed a set of greenish-gray and gray-black mudstone from a semi-shallow lake to a deep lake (Shang et al., 2011; Wang et al., 2011), is the main source rock of the Paleogene (Fig. 1c). Its sedimentary center is generally located in the North Tianshan piedmont thrust belt at the southern margin of the basin (Fig. 1b), and the thickness of the shale is generally about 50–200 m (Chen and Wang, 2004). The Cretaceous system consists of the Lower Cretaceous Qingshuihe Formation (K_{1q}), Hutubihe Formation (K_{1h}), Shengjinkou Formation (K_{1s}), Lianmuqin Formation (K_{1l}), and the Upper Cretaceous Donggou Formation (K_{2d}). The Lower Cretaceous K_{1q} developed a set of lacustrine deposition, is the main source rock of the Cretaceous (Wang et al., 2021) (Fig. 1c), and its sedimentary center is generally located in the piedmont thrust belt at the central and southern margin of the basin (Fig. 1b), with a maximum deposition thickness of approximately 250 m (Chen et al., 2015).

3. Samples and methods

3.1. Samples

In this study, 9 of the $E_{2\text{-}3a}$ samples were collected from the Anjihaihe outcrop (E85°61′, N44°62′) and DS Wells in the Junggar Basin, and 4 of the K_{1q} samples were collected from Sc and Pc Wells in the Junggar Basin, all experiments were carried out on the fresh surface of the sample to avoid the influence weathering and surface contamination. Petrological thin sections were prepared for all samples, and organic carbon (TOC), Rock pyrolysis (Rock-Eval), scanning electron microscopy (SEM), carbon isotope of kerogen ($\delta^{13}C_{kerogen}$), carbon isotope of a chloroform extract ($\delta^{13}C_{extract}$) and vitrinite reflectance (R_o) were measured. Furthermore, hydrous pyrolysis experiments were carried out for 4 typical samples,

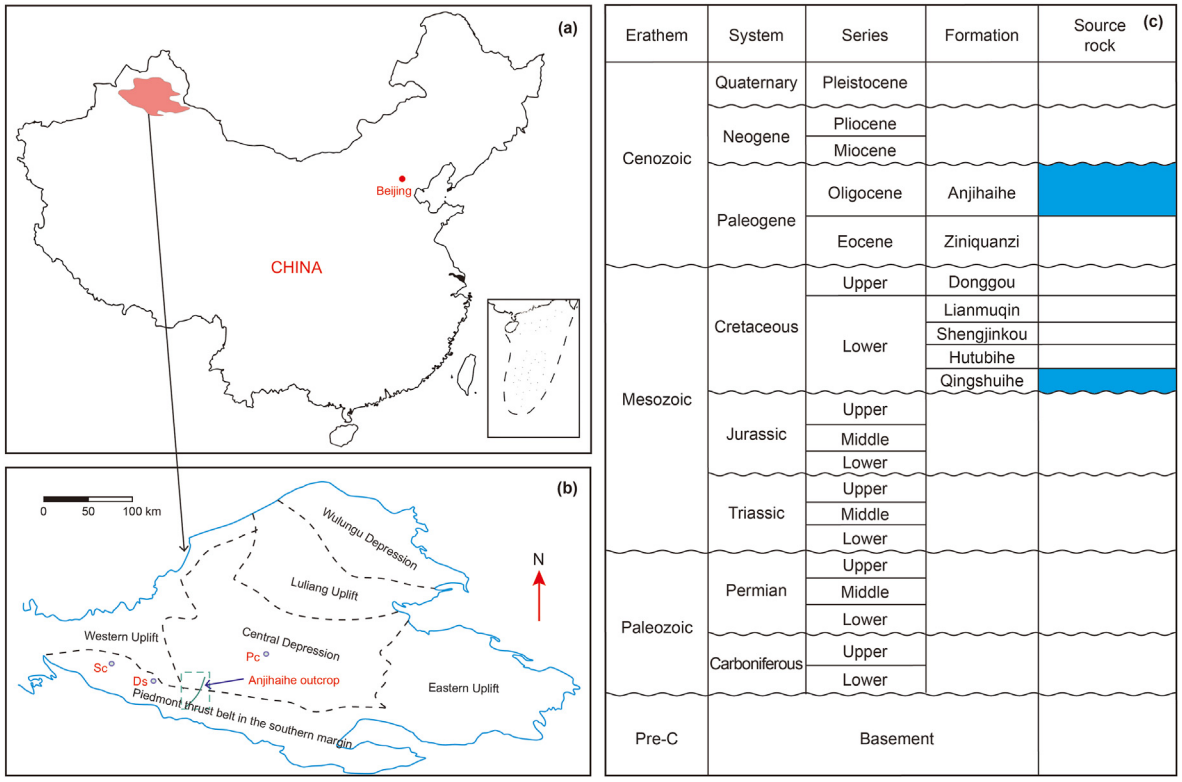

Fig. 1. Regional geological characteristics of the study area. Location of Junggar Basin, NW China (a); Location of the study area and tectonic structures of Junggar Basin (b); Stratigraphic column of the piedmont thrust belt in the southern margin of the Junggar Basin (c).

kinetic analysis was carried out for the 2 samples, and gas and liquid products were measured. The composition and carbon isotope of the gas products were also analyzed.

3.2. Methods

3.2.1. TOC analysis

Firstly, the sample was crushed to a particle size < 0.2 mm, and then about 100 mg of the sample was weighed into the crucible, and the inorganic carbon compounds were completely removed with 5% dilute hydrochloric acid. After that, the remaining sample was rinsed with distilled water for two days, at least 30 times, to ensure the removal of Cl ions and other impurities and prevent contamination of the instrument. After rinsing, the samples were put into the oven together with the crucible, and the samples were removed at a constant temperature of 60 °C for 12 h. The TOC content of the samples was determined by the LECO CS-230 carbon and sulfur analyzer under standard temperature and humidity. The main principle of determination is that OM is burned into carbon dioxide at a high temperature (> 800 °C), and then the amount of carbon dioxide is detected by an infrared detector and converted into a carbon element, and the content of organic carbon is calculated.

3.2.2. Rock-Eval pyrolysis analysis

Firstly, the samples were crushed to a particle size < 0.2 mm, and the pyrolysis parameters of the samples were determined using an OGE-II workstation at standard temperature and humidity. The initial temperature was 300 °C, and under anaerobic conditions, the sample was heated to 600 °C with nitrogen as carrier gas at a heating rate of 25 °C/min. The adsorbed hydrocarbon content (S_1), pyrolytic hydrocarbon content (S_2), and maximum pyrolysis temperature (T_{max}) of the samples were measured, and the hydrogen index (HI) and other parameters were calculated.

3.2.3. Organic petrographic

In this study, fluorescent thin sections of rocks were prepared for all samples to observe the morphology and type of OM in different samples. The thickness of the thin section was 0.05 mm, and there was no cover glass. It was particularly noted that the samples of the $E_{2\text{-}3a}$ of the Paleogene System were made of organic solvent as the medium because of their high clay content and strong water sensitivity, and the samples of the Cretaceous System were made of water medium. Leica DM4500P/DFC450C high-precision optical microscope was used as the observation instrument, and the maximum magnification of the objective lens was 50 times.

3.2.4. SEM analysis

The SEM can be used to observe the mineral composition and OM morphology of the sample. The observation sample is a minor core fracture, the surface is polished with argon ion, and the Au element is coated to improve the conductivity, thereby improving the observation clarity. Quanta 200F field emission scanning electron microscope was used for this observation, with a minimum resolution of 1.2 nm and magnification of 25000-200000.

3.2.5. Vitrinite reflectance (Ro) measurements

Organic petrological light slices were prepared for the original samples and hydrocarbon generation simulation residues for Ro determination. The instrument used is the MSP400 micro fluorescence spectrometer. Under the oil immersion objective lens, the intensity of the reflected light of the incident light within the limited area of the vitrinite profile with a photoelectric converter, and with the reflected light intensity of the reference material with known reflectivity under the same conditions. The specific operation process is carried out according to ASTM standard D7708-14 (2014). All tests were carried out under standard temperature and humidity.

3.2.6. Hydrous pyrolysis

The sample was crushed into a block with a size of about $2 \times 2 \times 2$ cm^3. In each experiment, 40 g of shales were loaded into the reactor. The reactor was closed and evacuated for several minutes before 10 mL of distilled water was injected into the reactor. GPM-3 hydrocarbon generation simulator was used to heat the sample to the set temperature at 2 °C/h, and the constant temperature is performed for 24 h. The rock samples were placed in reactors and analyzed according to the hydrocarbon generation characteristics of different samples. Aj1 and Aj2 samples were heated at 280 °C, 300 °C, 330 °C, 340 °C, 350 °C, 370 °C, 400 °C, 450 °Cand 500 °C, respectively. Sc samples were heated at 310 °C, 315 °C, 330 °C, 340 °C, 360 °C, 370 °C, 400 °C, 450 °C, and 500 °C, respectively. Pc1 samples were heated at 300 °C, 320 °C, 330 °C, 340 °C, 350 °C, 370 °C, 400 °C, 450 °C, and 500 °C. All experiments are conducted at standard temperature and humidity. The liquid hydrocarbon collected on the surface of the sample, the wall of the kettle, and the pipeline are regarded as the expelled oil, and the sample obtained by crushing and extracting is the residual oil. The collected gaseous hydrocarbon is analyzed by gas chromatography, the gas production is calculated according to the true gas state equation (Lewan et al., 2008), and the total hydrocarbon generation of the sample (liquid hydrocarbons + gaseous hydrocarbons) is finally obtained.

3.2.7. Kinetic analysis

Three parallel samples of 100 mg were prepared from each sample, and the analytical cycle of the Rock-Eval instrument was set for performing activation energy analysis. Specifically, the sample was set to be heated at a constant temperature of 200 °C for 5 min to remove adsorbed hydrocarbons and was then heated from 200 °C to 600 °C at a constant rate in different stages. Real-time records of the product quantity and hydrocarbon-generation conversion rate were collected under different conditions. According to the data recorded, the temperature versus hydrocarbon rate curve was mapped to calibrate the kinetic parameters during hydrocarbon generation, and the heating rate scheme of 15 °C/min, 25 °C/min, and 40 °C/min was adopted.

3.2.8. Expelled and residual oil

After the reaction, the expelled oil and residual oil, two organic phase products, can be collected in the reactor. The expelled oil mainly exists in the reactor in liquid form (Lewan, 1983), which can be directly washed out with CH_2Cl_2, then the rock cuttings are taken out, and the surface oil slick is soaked with CH_2Cl_2. After that, the reaction residue is crushed to 100 meshes and then extracted by the Soxhlet extractor method for 72 h until the residual oil in the reaction residue is completely extracted.

3.2.9. Carbon isotope analysis

All the powder samples (< 0.2 mm) were extracted by the Soxhlet extraction method, and the $\delta^{13}C_{extract}$ was determined. Kerogen was prepared from all samples and $\delta^{13}C_{kerogen}$ was determined. The gas products generated at each simulated temperature are collected by the drainage gas gathering method, and the carbon isotope of the gases is measured separately. The test instrument is Trace GC-ISO LINK-MAT 253 IRMS mass spectrometry linked gas chromatograph, and the specific operation was carried out according to SY/T 5238–2019.

3.2.10. Chemical composition analysis of gases

The chemical composition of the gas generated at each simulated temperature was determined. Agilent 6890 four-valve, five-column multidimensional gas chromatograph was used as the test instrument. The temperature of TCD and FID detectors was 250 °C, the initial column temperature was 50 °C, and the temperature was kept for 3 min. The temperature was raised to 100 °C at 5 °C/min and then to 180 °C at 10 °C/min, and the temperature was maintained for 3 min. Specific operations were carried out according to GB/T 13610–2014.

4. Results and discussion

4.1. Organic petrology and SEM

Through organic petrology and SEM, *Pediastrum* (Fig. 2a) was identified in the $E_{2\text{-}3a}$ shale samples of Junggar Basin for the first time; it is widely distributed, complete in shape, and generally star-shaped, with narrow and long cells, clear structure, large perforation, yellow-green orange fluorescence, and a diameter of 30 μm–50 μm (Fig. 2b). *Pediastrum* belongs to Chlorophyta, Hydroreticulae (Komárek and Jankovská, 2001; Geel, 2001; Zamaloa and Tell, 2005; Weckström et al., 2010). The outer layer of its cell wall is composed of sporopollenin and silicon oxide, which has strong corrosion resistance, so its fossils can be well preserved in sediments (Jankovsk and Komárek, 2000; Komárek and Jankovská, 2001; Weckström et al., 2010), and it is widely distributed throughout the world. *Pediastrum* is a good hydrocarbon-generating OM, equivalent to type I kerogen, and one of the original materials providing effective oil generation in the geological age (Hutton, 1987; Wang et al., 1994). In this study, *Oscillatoria* (cyanobacteria) was firstly identified in the K_{1q} shale of Junggar Basin (Fig. 2), which is also widely distributed, but its diameter is small, mainly distributed in 5 μm (Fig. 2c); it is mainly characterized by densely stacked layers, almost no recognizable structure, high translucency, indistinguishable from the mineral matrix under normal reflected light, and easy to identify under intense fluorescence irradiation (Stach et al., 1982; Taylor et al., 1998). Cyanobacteria is the only prokaryote that conducts photosynthesis among much lower aquatic plankton. *Oscillatoria* belongs to Oscillatoriaceae, Cyanophyt; it is the first organism that generates oxygen through photosynthesis. It is one of the oldest plant groups on the earth and plays a vital role in the process of biological evolution. Because they are rich in protein and lipid, they are considered potential precursors of OM in hydrocarbon source rocks (Douglas et al., 1991; Schidlowski et al., 1992).

Both green algae and cyanobacteria are layered in the vertical bedding direction, and the bedding development is obvious (Fig. 2d-f). The difference is that the individual green algae are relatively independent, while the individual cyanobacteria are closely interbedded with the mineral matrix. This discovery implies that although the $E_{2\text{-}3a}$ shale and the K_{1q} shale in the Junggar basin are lacustrine sediments, they have entirely different hydrocarbon-generating OM. The algal precursor of the $E_{2\text{-}3a}$ shale is *Pediastrum* of Chlorophyceae, which is more consistent with the Rundle type shale (Hutton, 1987), while the kerogen precursor of the K_{1q} shale is mainly cyanobacteria, which is more consistent with the Alberta shale in Canada (Smith et al., 1991) and the Upper Paleozoic hydrocarbon source rock of the Timan Pechora basin in Russia (Collister et al., 2004). Because the evolution mechanism of kerogen controls the generation process of hydrocarbons (Loucks et al., 2009), the hydrocarbon generation characteristics of the two sets of lacustrine shale may also be different.

4.2. Organic geochemical characteristics of unheated samples

The TOC of $E_{2\text{-}3a}$ shale rich in green algae ranged from 0.57% to 2.70% (avg. 1.38%) (Table 1), $S_1 + S_2$ ranged from 0.65 mg/g to

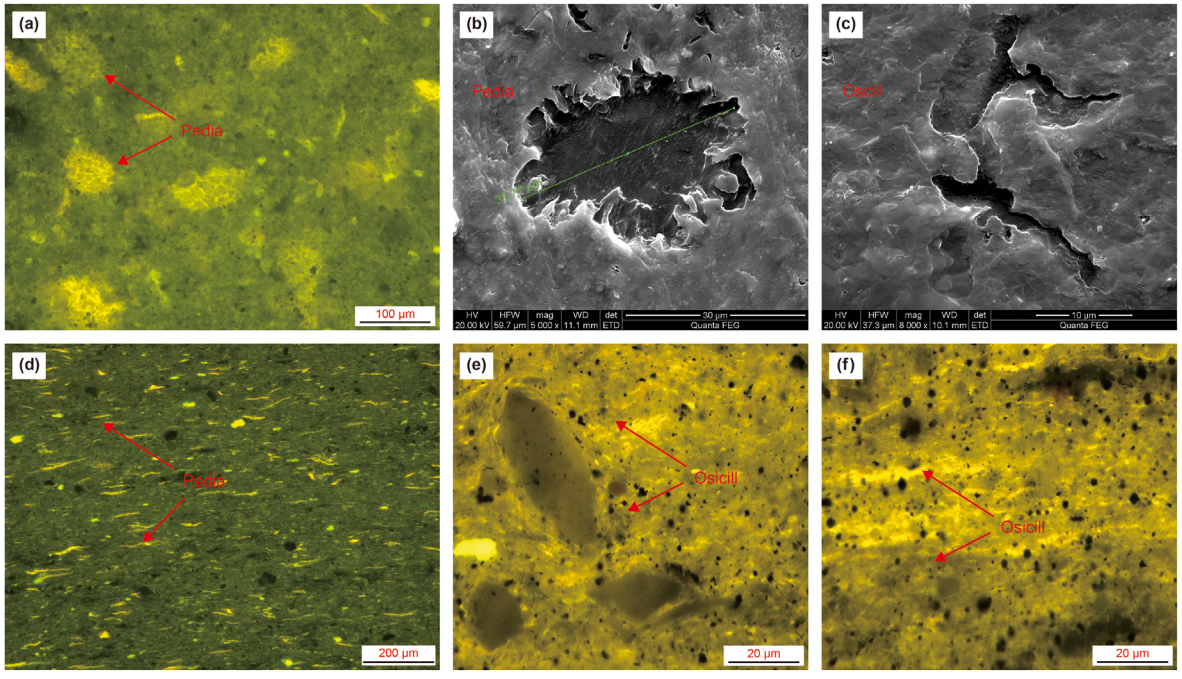

Fig. 2. Organic petrology and SEM images of the samples. Image of parallel bedding direction section of sample rich in *Pediastrum* (a); SEM image of sample rich in *Pediastrum* (b); SEM image of sample rich in *Oscillatoria* (c); Image of vertical bedding section of sample rich in *Pediastrum* (d); Image of vertical bedding section of sample rich in *Oscillatoria* (e and f)
Abbreviations: Pedia, *Pediastrum*; Oscicill, *Oscillatoria*.

Table 1
Organic geochemical characteristics of unheated samples parameters.

Group	Samples	TOC, %	S_1, mg HC/gRock	S_2, mg HC/gRock	T_{max}, °C	PG, mg HC/gRock	HI, mg HC/gTOC	R_o, %	Algae
$E_{2\text{-}3a}$	AJ1	2.70	0.24	16.98	439	17.22	628	0.65	Green algae
$E_{2\text{-}3a}$	AJ2	1.34	0.24	10.19	436	10.43	763	0.66	Green algae
$E_{2\text{-}3a}$	AJ3	1.19	0.17	5.82	436	5.99	490	0.69	Green algae
$E_{2\text{-}3a}$	AJ4	2.26	0.21	12.37	439	12.58	548	0.66	Green algae
$E_{2\text{-}3a}$	AJ5	1.90	0.36	10.64	434	11	561	0.7	Green algae
$E_{2\text{-}3a}$	AJ6	1.94	0.25	10.75	436	11	554	0.71	Green algae
$E_{2\text{-}3a}$	AJ7	0.77	0.14	2.78	433	2.92	361	0.73	Green algae
$E_{2\text{-}3a}$	AJ8	1.29	0.48	6.10	433	6.58	473	0.67	Green algae
$E_{2\text{-}3a}$	DS	0.57	0.48	1.97	432	2.45	349	0.61	Green algae
K_{1q}	SC	2.23	0.52	14.05	435	14.57	630	0.52	Cyanobacteria
K_{1q}	PC1	1.17	0.41	6.88	435	7.29	587	0.61	Cyanobacteria
K_{1q}	PC2	0.96	0.13	4.78	443	4.91	499	0.63	Cyanobacteria
K_{1q}	PC3	1.04	0.22	4.07	444	4.29	392	0.57	Cyanobacteria

Note:TOC: total organic carbon, w.t.%; S_1: residual hydrocarbon, mg HC/g rock; S_2: pyrolysis hydrocarbon, mg HC/g rock; PG=S_1+S_2: hydrocarbon potential, mg HC/g rock; HI: hydrogen index = 100 × S_2/TOC, mg HC/g TOC; T_{max}: peak temperature of pyrolysis, °C; R_o: vitrinite reflectance, %R_o.

17.22 mg/g (avg. 7.00 mg/g), TOC of cyanobacteria-rich samples ranged from 0.96% to 2.23% (avg. 1.35%) (Table 1). $S_1 + S_2$ ranged from 4.29 mg/g to 14.57 mg/g (avg. 7.77 mg/g), indicating strong heterogeneity. Both green algae-rich and cyanobacteria-rich samples showed good hydrocarbon generation potential (Fig. 3a and b) (Peters, 1986).

The rock pyrolytic hydrogen index (*HI*=S_2 × 100/TOC) is often used to evaluate the type of OM in source rocks (Espitalie et al., 1985). The *HI* values of $E_{2\text{-}3a}$ shale samples rich in green algae ranged from 349 to 763 (mg HC/g TOC) (avg. 525 mg HC/g TOC). The *HI* of K_{1q} shale samples rich in cyanobacterial ranged from 392 (mg HC/g TOC) to 630 (mg HC/g TOC) (avg. 527 mg HC/g TOC), and the OM types were mainly typed I and typed II (Fig. 3c) (Mukhopadhyay et al., 1995). Rock pyrolysis and vitrinite reflectance methods are commonly used to evaluate OM maturity (Lafargue et al., 1998; Hakimi and Hasiah, 2013), T_{max} of the two types of samples is distributed at about 435 °C, the R_o is between 0.52% and 0.73% (avg. 0.65%), and OM is in the low maturity–mature stage.

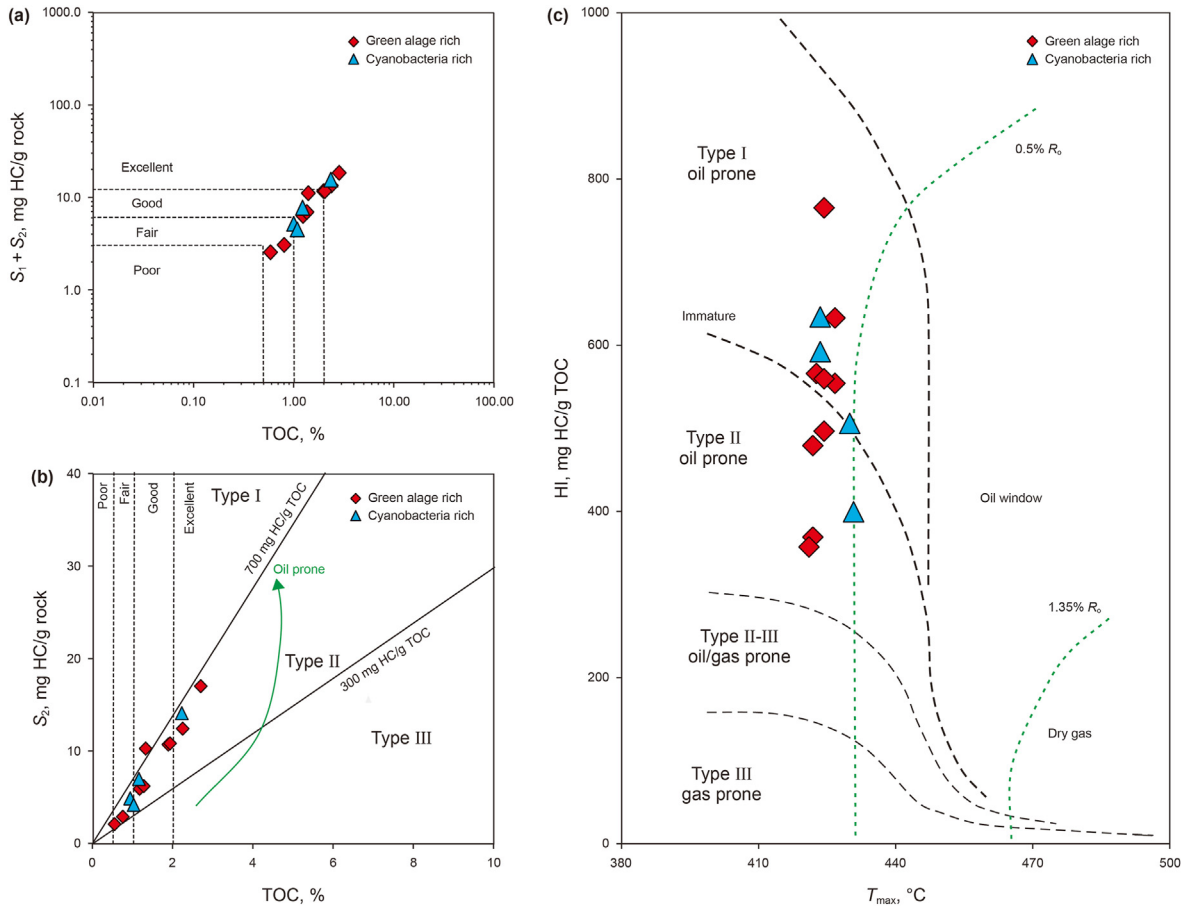

Fig. 3. Plot of Generative Potential ($S_1 + S_2$) vs. Total Organic Carbon content (TOC) (a) (according to Peters, 1986); Plot of S_2 vs. Total Organic Carbon content (TOC) (b) (according to Peters, 1986); *HI* vs. T_{max} (c) (according to Mukhopadhyay et al., 1995).

4.3. Hydrous pyrolysis and kinetic analysis

Based on the results of organic geochemical analysis and organic petrology analysis, Aj1 and Aj2 of the $E_{2\text{-}3a}$, two typical samples rich in green algae, and Sc and Pc1 of the K_{1q}, two samples rich in cyanobacteria, were selected for the hydrous pyrolysis, and the yields of liquid and gaseous hydrocarbons were obtained in (Table 2). The results show that the hydrocarbon generation characteristics of Aj1 and Aj2 are relatively consistent (Fig. 4a and b). Both of them reach the oil generation peak at the simulated temperature of 350 °C, and the maximum oil generation is 401 mg/g [TOC] and 320 mg/g[TOC], respectively. The total liquid hydrocarbon production rate is consistent with the expelled oil production peak. Aj1 and Aj2 have high residual hydrocarbon production rates. With increasing simulated temperature, Aj1 and Aj2 residual hydrocarbon production rates slowly decrease, and the residual hydrocarbon production rates only decrease significantly at 400 °C, which may be related to the mineral composition. The high content of clay minerals has a strong adsorption effect on the retained hydrocarbons (Klewiah et al., 2019), Aj1 and Aj2 contain a large number of clay minerals, and the content of clay minerals can reach about 60%, which may be one of the reasons for limiting the discharge of crude oil. In addition, it may be related to the OM composition. Wang et al. (1994) conducted pyrolysis experimental research on *Pediastrum* and found that the liquid hydrocarbon generated from it is rich in heavy components such as resins and asphaltene (Wang et al., 1994), and the content of resins + asphaltene can reach 90%, while the asphaltene has a significant polarity and is easily adsorbed by kerogen into retained oil (Lewan et al., 1979; Sandvik et al., 1992; Ritter, 2003). It is worth noting that Aj1 and Aj2 begin to generate hydrocarbons at relatively low temperatures, with large amounts of liquid hydrocarbons being generated at 280 °C (179.3 mg/g[TOC] and 189.55 mg/g[TOC], respectively), suggesting that Aj1 and Aj2 can even generate liquid hydrocarbons at earlier stages. Therefore, Aj1 and Aj2, represented by green algae, may have a wide oil generation window, which may be a typical feature of Aj1 and Aj2. However, the residual oil is the primary hydrocarbon generated at low temperatures, and then the liquid hydrocarbon production rate increases slowly.

The typical characteristics of Sc and Pc1, which are rich in cyanobacteria, began to generate oil after the simulated temperature of 300 °C and reached the oil peak at about 340 °C. The maximum oil generation at the oil peak was 677 mg/g[TOC] and 328 mg/g[TOC], respectively. This may be related to the difference in enrichment and preservation of cyanobacteria caused by changes in the sedimentary environment, which can also be reflected in their respective OM abundance (Fig. 3a; Table 1), but their overall evolution trend is similar. Pc1 and Sc have very different hydrocarbon generation characteristics from Aj1 and Aj2. Pc1 and SC started oil generation later but reached the oil generation peak earlier, which is manifested as a narrow oil generation window and relatively concentrated hydrocarbon generation. Jin (2000) conducted a comparative experiment on the hydrous pyrolysis of pollen and algae, and the experimental data are shown in Table 3. Due to the

Table 2
Hydrocarbon pyrolysis yields at different temperatures.

Formation	Samples	Temperature, °C	R_o, %	Sample weight, g	Expelled oil, mg/g·TOC	Residual oil, mg/g·TOC	Hydrocarbon gas, mg/g·TOC	Liquid hydrocarbon, mg/g·TOC	Total hydrocarbon, mg/g·TOC
$E_{2\text{-}3a}$	Aj1	280	0.68	40	44.87	134.44	9.15	179.30	188.45
		300	0.69	40	82.54	140.64	3.17	223.17	226.34
		330	0.75	40	164.13	142.21	11.08	306.34	317.42
		340	0.76	40	214.24	151.13	20.42	365.38	385.79
		350	0.84	40	257.86	143.76	36.27	401.62	437.90
		370	0.96	40	205.73	138.65	139.22	344.39	483.61
		400	1.11	40	97.51	84.57	378.78	182.08	560.86
		450	1.27	40	23.71	70.60	507.71	94.31	602.02
		500	1.49	40	13.70	34.82	660.66	48.51	709.17
	Aj2	280	0.69	40	51.65	137.90	9.26	189.55	198.81
		300	0.72	40	70.55	136.49	19.46	207.03	226.49
		330	0.75	40	130.07	128.76	45.76	258.83	304.59
		340	0.78	40	170.04	126.70	70.13	296.75	366.87
		350	0.84	40	208.91	111.11	95.64	320.02	415.66
		370	0.93	40	184.73	95.49	161.28	280.22	441.50
		400	0.99	40	89.26	61.79	325.96	151.05	477.01
		450	1.21	40	67.74	52.33	434.56	120.07	554.63
		500	1.55	40	25.64	14.07	598.71	39.70	638.41
K1tg	Sc	310	0.60	40	26.23	16.08	1.91	42.31	44.22
		315	0.67	40	69.17	34.91	5.72	104.08	109.80
		330	0.73	40	369.39	95.74	10.64	465.14	475.77
		340	0.80	40	660.58	104.73	17.37	765.31	782.68
		360	0.94	40	597.80	79.88	100.37	677.68	778.05
		370	1.12	40	336.51	73.62	355.22	410.13	765.35
		400	1.23	40	207.89	20.54	548.64	228.43	777.07
		450	1.34	40	39.69	26.68	745.68	66.36	812.04
		500	1.41	40	34.42	22.64	817.14	57.05	874.19
	Pc	300	0.67	50	73.55	17.30	4.11	90.85	94.96
		320	0.71	50	232.94	32.41	6.07	265.35	271.42
		330	0.74	50	267.24	35.15	6.70	302.39	309.09
		340	0.80	50	284.13	44.35	11.19	328.48	339.67
		350	0.94	50	225.94	54.39	80.19	280.33	360.52
		370	1.10	50	151.45	38.33	265.74	189.78	455.52
		400	1.20	50	46.42	33.61	433.97	80.03	514.00
		450	1.29	50	22.87	21.36	529.45	44.22	573.67
		500	1.43	50	5.29	21.27	630.51	26.56	657.07

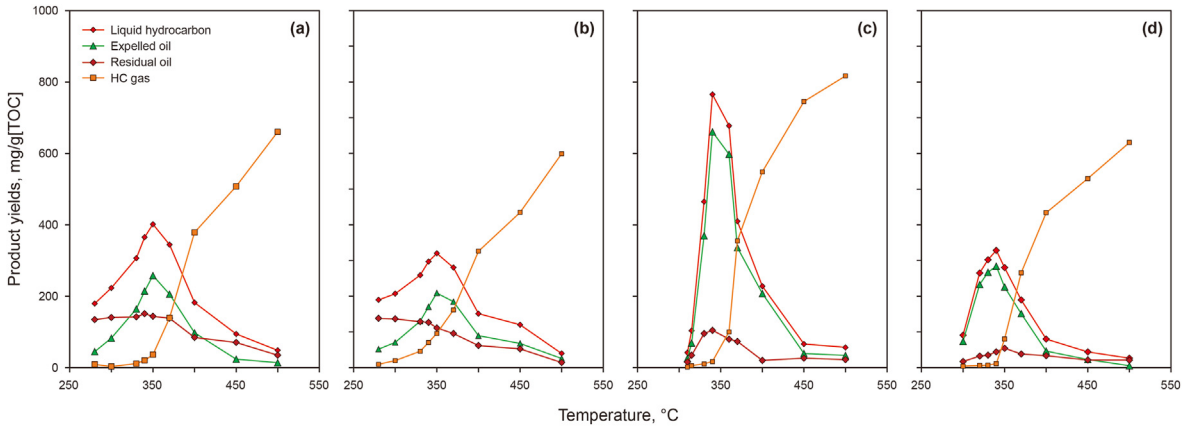

Fig. 4. Hydrous pyrolysis yields for the green algae-rich samples of the $E_{2\text{-}3a}$ and the cyanobacteria-rich samples of the K_{1q}. Hydrocarbon generation evolution of sample Aj1 rich in green algae from the $E_{2\text{-}3a}$ (a); Hydrocarbon generation evolution of sample Aj2 rich in green algae from the $E_{2\text{-}3a}$ (b); Hydrocarbon generation evolution of sample Sc rich in Cyanobacteria from the K_{1q} (c); Hydrocarbon generation evolution of sample Pc1 rich in Cyanobacteria from the K_{1q} (d).

Table 3
Hydrocarbon pyrolysis yields at different temperatures (Data is from Jin, 2000).

Samples	Temperature, °C	Hydrocarbon gas, mg/g·TOC	Liquid hydrocarbon, mg/g·TOC	pH of water
a	190	72.45	15.06	7.5–8
	230	116.6	18.81	7.5–8
	280	124	53.66	8.5
	300	155.57	60.53	8.5–9
	320	206	48.36	8.5–9
	360	373.11	17.05	8.5–9
b	140	27.59	6.87	7
	180	88	19.77	8–8.5
	230	121.76	23.84	8.5
	280	139.76	40.5	8.5–9
	300	142.8	89.69	8.5–9
	320	160.5	52.56	8.4–9
	350	202.8	47.64	8.5–9
	365	237.8	46.44	8.4–9
	395	348	34.08	8.5–9

differences in experimental conditions and instruments, the peak temperature of oil generation and the maximum amount of hydrocarbon generation are different to some extent. However, the experiment also showed that the sample rich in green algae had a wide oil generation window, and the oil generation peak was not obvious (Fig. 5a). However, the samples rich in cyanobacteria showed an obvious oil generation peak (Fig. 5b), which was consistent with the results of this comparative experiment.

In this study, the vitrinite reflectance R_o of four typical samples at different simulated temperature points was measured, and the hydrocarbon yield models of cyanobacteria-rich shale and green algae-rich shale were established, respectively (Fig. 6). The initial R_o of all samples is between 0.5% and 0.7%, and all samples are low maturity, so they can reflect a relatively complete hydrocarbon generation evolution process. When R_o is about 0.68%, the total hydrocarbon yield of Aj1 and Aj2 was 188.45 mg/g[TOC] and

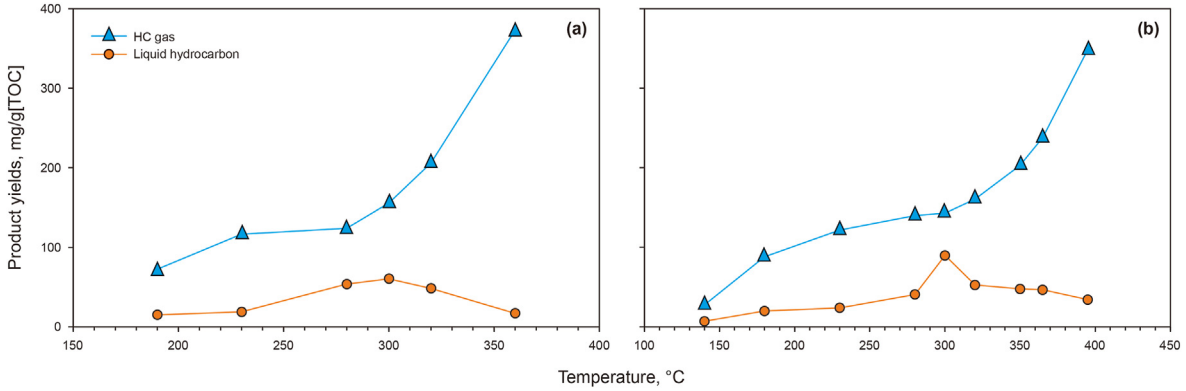

Fig. 5. Hydrous pyrolysis simulation experiment results from Jin (2000). Hydrocarbon generation evolution of samples rich in green algae (a); Hydrocarbon generation evolution of samples rich in cyanobacteria (b).

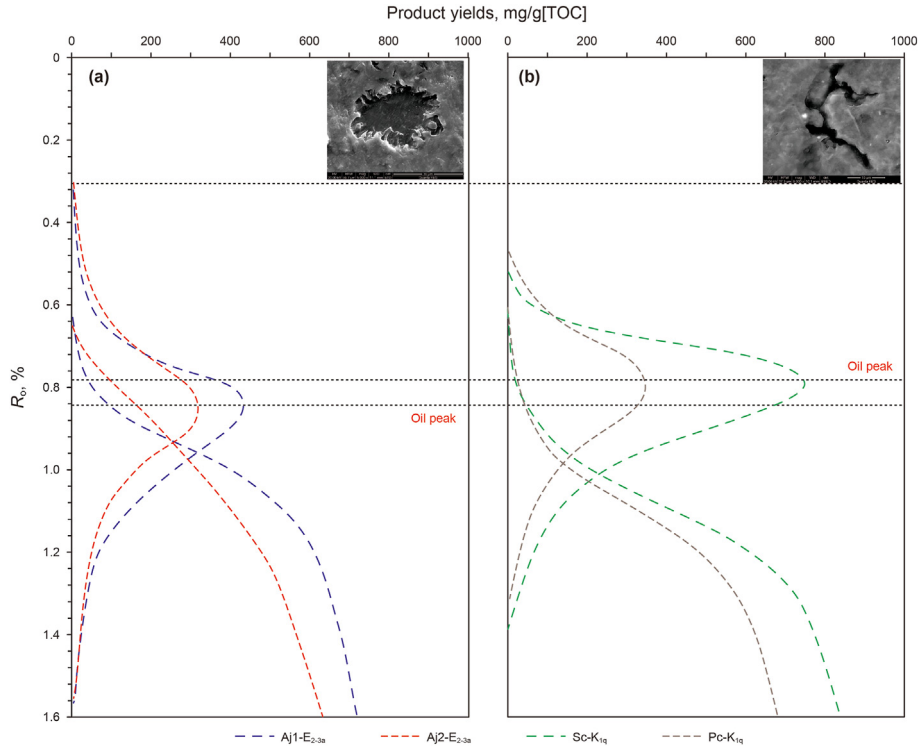

Fig. 6. Patterns of yield for green algae-rich and cyanobacteria-rich samples. Plot of hydrocarbon generation yield of a green algae-rich sample (a); Plot of hydrocarbon generation yield of a cyanobacteria-rich sample (b).

198.81 mg/g[TOC], respectively, and then reached the peak of liquid hydrocarbon yield at about 0.84% R_o. However, the total hydrocarbon yields of Sc and Pc1 were 109.8 mg/g[TOC] and 94.96 mg/g [TOC], respectively, and reached the peak of liquid hydrocarbon yield at R_o of 0.80% (Fig. 6), which was consistent with the product evolution trend corresponding to the simulated temperature.

The difference in hydrocarbon generation mechanism between green algae and cyanobacteria may be related to the activation energy of the kerogen reaction. The essence of kerogen cleavage and hydrocarbon generation is a series of chemical bond-breaking processes, and the evolution mechanism of kerogen controls the hydrocarbon generation process and hydrocarbon generation mode (Loucks et al., 2009). As for the dynamic mechanism of different types of kerogens that evolve for the generation of hydrocarbons, the opinions vary among scholars (Tissot, 1978; Quigley and Mackenzie, 1988). Some scholars believed that the time sequence for hydrocarbon generation by kerogen is as follows: Type I kerogen > Type II kerogen > Type III kerogen (Schenk et al., 1997). However, some researchers believe that the activation energy of different types of kerogens required for the generation of hydrocarbons has a sequence of EII < EI < EIII (EI: activation energy of Type I kerogen) (Tissot et al., 1987). Even for the same type of kerogen, the activation energy characteristics will be significantly different (Peters et al., 2006). At this time, the hydrocarbon generation of OM depends on its chemical structure and material composition (Rullkotter et al., 1987; Schenk et al., 1997; Primio et al., 2000). The fluorescence of cyanobacteria represents homogeneity whereas that observed in the middle of green algae and around it exhibits evident differences (Fig. 2). This also reflects that the chemical composition of cyanobacteria is simple, whereas a significant chemical heterogeneity is observed in the case of green algae. Therefore, the activation energy of green algae during degradation and hydrocarbon generation is wide and that of cyanobacteria is narrow.

The activation energy distribution of green algae was relatively wide, within the range of 230–385 kJ/mol, with an average activation energy of 323 kJ/mol (Fig. 7a) (Table 4). Conversely, the activation energy distribution of cyanobacteria is relatively concentrated, within the range of 246–380 kJ/mol, with an average activation energy of 295 kJ/mol (Fig. 7b) (Table 4). This indicates that the hydrocarbon generation of green algae is characterized by lower initial hydrocarbon-generation activation energy and wide activation energy distribution, whereas that of cyanobacteria is characterized by a higher initial hydrocarbon-generation activation energy and a narrow activation energy distribution. The central frequency of activation energy varies significantly among different types of kerogens (Picard, 1985; Primio et al., 2000), and the differential evolution of kerogen is related to the kerogen precursor (Smith et al., 1991; Dieckmann et al., 2006). *Pediastrum* and *Oscillatoria* have completely different precursors, which is the fundamental reason for the difference in hydrocarbon generation characteristics between the E_{2-3a} *Pediastrum*-rich and the K_{1q} *Oscillastoria*-rich shales.

4.4. Characteristics of crude oil components evolution

The hydrocarbon generation characteristics of the E_{2-3a} green algal-rich shale and the K_{1q} cyanobacteria-rich shale are pretty different, and their initial oil generation time, oil generation peak, and maximum oil generation are significantly different, which are not only apparent in the yield diagram (Fig. 4), but also well reflected in the liquid hydrocarbon group components at different pyrolysis temperatures. Ruble et al. (2003) found that the content of heavy components (resins + asphaltene) in crude oil was the highest at and near the peak of oil generation in the hydrous pyrolysis experiment of Green River shale. This means that group component separation will also occur in the process of hydrocarbon generation (Han et al., 2015). Lin et al. (2022) also obtained the

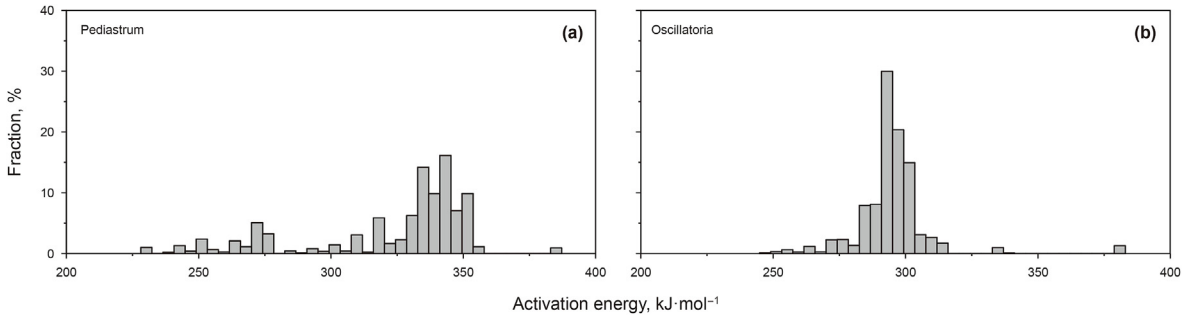

Fig. 7. Activation energy distribution and frequency factors of green algae and cyanobacteria. Activation energy distribution and frequency factor of green algae (*Pediastrum*) (a); Activation energy distribution and frequency factor of cyanobacteria (*Oscillatoria*) (b).

Table 4
Hydrocarbon generation rate and activation energy data distribution data.

Activation energies, kJ/mol	Hydrocarbon generation rate, %-Sc	Hydrocarbon generation rate, %-Aj1
230–240	0	1.24
240–250	0.12	1.72
250–260	1.24	3.30
260–270	1.48	3.24
270–280	4.57	8.32
280–290	17.36	0.54
290–300	50.4	1.19
300–310	20.73	4.94
310–320	1.73	6.13
320–330	0	3.92
330–340	1.06	30.3
340–350	0	23.2
350–360	0	11.02
360–370	0	0
370–380	0	0
380–390	1.31	0.94

same conclusion when studying the organic-rich oil shale of the Lower Permian in Tasmania, Australia. That is, with the increase of thermal simulation temperature, the relative content of saturated hydrocarbons and aromatic hydrocarbons in expelled oil and residual oil decreased first and then increased, while the content of resins and asphaltene increased first and then decreased (Fig. 8) (Table 5) (Lin et al., 2022; Gao et al., 2023). This trend may be due to the formation of large molecular hydrocarbons such as resins and asphaltene in the early stage of thermal evolution, and in the middle and late stages of thermal evolution, they gradually split into saturated hydrocarbons and aromatic hydrocarbons.

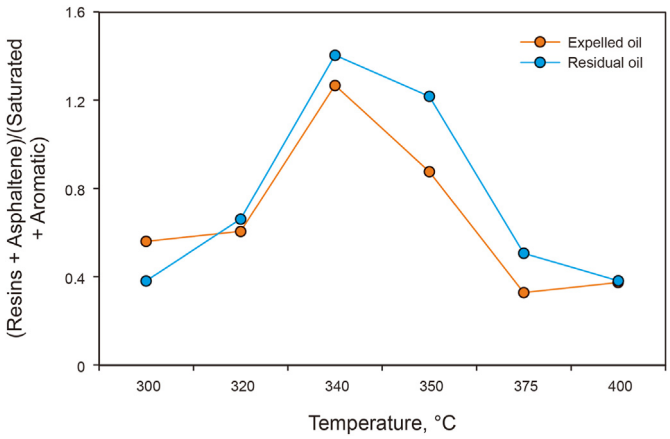

Fig. 8. Relationship between liquid product group component content and thermal evolution degree of the Lower Permian organic-rich oil shale in Tasmania, Australia (Data is from Lin et al., 2022).

In this study, similar phenomena also occurred in the hydrous pyrolysis of the $E_{2\text{-}3a}$ shale rich in green algae and the K_{1q} shale rich in cyanobacteria. The components were separated from the residual oil of Sc and Aj1 at different pyrolysis temperatures, and the results are shown in Table 6, which are consistent with the research conclusions of Ruble et al. (2003). At low simulated temperatures, green algae can already generate heavy crude oil (high content of resins + asphaltene). After that, the relative content of heavy components does not change significantly. At about 340–350 °C, the ratio of (resins + asphaltene)/(saturated + aromatic) reaches the highest value, about 2.27–2.30 (Fig. 9a). However, the oil generation peak of cyanobacteria was more prominent, and the time of a large amount of oil generation was relatively late, reaching the peak value of about 1.37 at 340 °C (Fig. 9b). It can be seen from this that the $E_{2\text{-}3a}$ green algae rich shale have a low threshold and heavy oil quality, which is more consistent with the research conclusion of Wang et al. (1994). However, in Wang et al. (1994)'s experiment, the content of heavy components of oil generated by *Pediastrum* (green algae) is higher, while the K_{1q} cyanobacteria-rich shale has a late oil generation time, relatively concentrated hydrocarbon generation and relatively light oil quality.

The answer can also be obtained intuitively from the images of residual oil corresponding to different pyrolysis temperatures (Fig. 9c). From left to right, the images of residual oil of green algae at 300 °C, 330 °C, 340 °C, 350 °C, 370 °C, 400 °C, 450 °C and 500 °C are shown in sequence (Fig. 9d). From left to right, the residual oil images of cyanobacteria at 310 °C, 315 °C, 330 °C, 340 °C, 360 °C, 370 °C, 400 °C, 450 °C, and 500 °C are shown. It is generally

Table 5
Composition of residual oil compounds produced during hydrous pyrolysis experiments (Data is from Lin et al., 2022).

Samples	Temperature, °C	Saturated hydrocarbon, %	Aromatic hydrocarbon, %	Resins, %	Asphaltene, %	(Resins + asphaltene)/(Saturated + aromatic)
Expelled oil	300	31.6	32.5	24.3	11.6	0.56
	320	25.9	36.4	22.5	15.2	0.61
	340	18.4	25.7	21.1	34.8	1.27
	350	23.1	30.2	24.9	21.8	0.88
	375	38.9	36.4	14.9	9.8	0.33
	400	8.4	64.4	16.8	10.4	0.37
Residual oil	300	14.6	57.8	19.5	8.1	0.38
	320	9.6	50.6	23.5	16.3	0.66
	340	6.1	35.5	30.0	28.4	1.40
	350	7.9	37.2	30.4	24.5	1.22
	375	12.0	54.4	16.0	17.6	0.51
	400	14.7	57.7	19.5	8.1	0.38

Table 6
Composition of residual oil compounds produced during hydrous pyrolysis experiments.

Samples	Temperature, °C	Saturated hydrocarbon, %	Aromatic hydrocarbon, %	Resins, %	Asphaltene, %	(Resins + asphaltene) /(Saturated + aromatic)
Sc	310	35.8	35.0	25.6	3.7	0.41
	315	33.2	33.1	24.1	9.6	0.51
	330	34.7	27.5	25.4	12.4	0.61
	340	22.6	19.6	31.1	26.7	1.37
	360	34.4	23.9	26.0	15.7	0.72
	370	37.7	27.2	24.7	10.4	0.54
	400	27.5	38.5	24.6	9.4	0.51
	450	33.7	34.4	20.7	11.2	0.47
	500	32.5	40.7	17.7	9.1	0.37
Aj1	280	20.5	16.7	34.6	28.2	1.69
	300	18.4	17.4	35.2	29.0	1.79
	330	19.5	15.4	32.4	32.7	1.87
	340	19.6	10.7	29.3	40.4	2.30
	350	13.2	17.4	24.6	44.8	2.27
	370	19.9	15.7	26.1	38.3	1.81
	400	25.6	25.5	27.7	21.1	0.96
	450	39.8	28.2	21.5	10.5	0.47
	500	43.7	25.5	17.9	12.9	0.45

believed that the resins and asphaltene in crude oil components are dark and brown-black, while the saturated hydrocarbon is colorless, and the aromatic hydrocarbon is generally light yellow. The results of this experiment have apparent regularity; at the peak of oil generation, the residual oil of either cyanobacteria or green algae has the deepest color (Fig. 9c and d). From the low-temperature stage of pyrolysis to the peak of oil generation, the color of green algae changes in sequence (Fig. 9c), which is also evidence of its earlier oil generation and heavier oil quality. The characteristics of the oil generation of cyanobacteria are most evident in the images. The residual oil at the peak of oil generation is almost black (Fig. 9d), which is another manifestation of its narrow oil window and concentrated oil generation.

4.5. Characteristics of carbon isotopes

Fenton and Ritz (1989) study of carbon isotopes in modern macroalgae found that the $\delta^{13}C_{kerogen}$ of benthic algae was generally less than −30‰, with an average of −33.5‰ (Fenton and Ritz, 1989). Brutemark et al. (2009) analyzed the $\delta^{13}C_{kerogen}$ of planktic algae and showed that the $\delta^{13}C_{kerogen}$ of planktic algae was generally heavier than −30‰ (Brutemark et al., 2009), the faster the growth rate of planktic algae, the less fractionates carbon isotopes, and the heavier carbon isotopes (Laws et al., 1995). Carbon sources in water mainly include atmospheric CO_2, dissolved CO_2 and HCO_3^- in water, and CO_2 and HCO_3^- released after plant corruption. Carbon isotopes of CO_2 in the atmosphere and CO_2 and HCO_3^- formed from its direct dissolution are relatively heavy, while carbon isotopes of CO_2 and HCO_3^- released from plant decay after plant absorption and fractionation are relatively light (Jones et al., 2010). Therefore, if the fractionation intensity is consistent, the utilization ratio of the carbon source may be different, which may be an essential reason for the difference in the carbon isotope weight of algae. Maberly et al. (1992) calculated that the carbon isotope of HCO_3^- on the surface of modern seawater is about 0, and believed that for algae with only atmospheric CO_2 and HCO_3^- formed by its direct dissolution as the carbon source, its $\delta^{13}C_{kerogen}$ is generally higher than −30‰. In addition, the carbon fixation process of photosynthesis is also an important factor affecting the carbon isotope of algae. The less carbon leakage in this process, the heavier the carbon isotope of algae (Sharkey and Berry, 1986). Natural gas generated by pyrolysis is generally divided into two sources, namely, kerogen-cracked gas and crude oil-cracked gas, whose carbon isotopes are relatively stable. However, in the pyrolysis process, due to the constant changes in the properties of reactants and the types of chemical bond breaks, the hydrocarbon generation process is accompanied by isotope fractionation (Stahl, 1974; Ungger and Pelet, 1987). The distribution of carbon isotopes of gases at different temperatures during pyrolysis is shown in Table 7. Generally speaking, during pyrolysis, carbon isotopes of gaseous hydrocarbons first become heavier and then lighter as the simulated temperature increases (Tang et al., 2000; Dieckmann et al.,

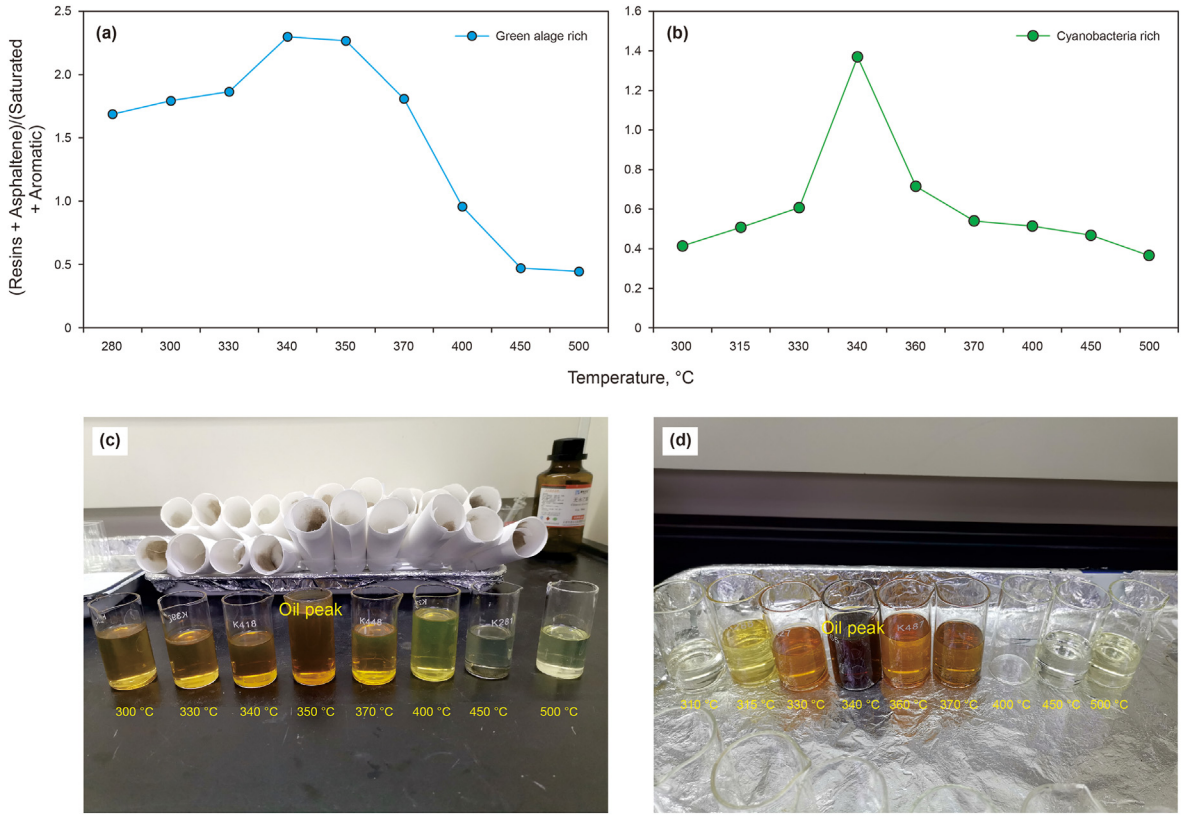

Fig. 9. Evolution characteristics of residual oil components in the $E_{2\text{-}3a}$ samples rich in green algae (a); Evolution characteristics of residual oil fractions in the K_{1q} samples rich in cyanobacteria (b); Color variation of residual oil in the $E_{2\text{-}3a}$ samples rich in green algae (c); Color variation of residual oil in the K_{1q} cyanobacteria-rich samples (d).

2006; Lewan and Roy, 2012), and the results of this study also showed a similar trend.

The $E_{2\text{-}3a}$ Shale rich in green algae $\delta^{13}C_{kerogen}$ is between −26.11‰ and −22.82‰ (avg. −24.29‰), $\delta^{13}C_{extract}$ is between −28.39‰ ~ −25.09‰ (avg. −26.95‰), the K_{1q} rich in cyanobacteria shale $\delta^{13}C_{kerogen}$ is between −29.72‰ and −26.94‰ (avg. −28.60‰), $\delta^{13}C_{extract}$ is between −31.36‰ and −29.54‰ (avg. −30.18‰) (Fig. 10) (Table 8). Whether the $E_{2\text{-}3a}$ shale is rich in green algae or the K_{1q} shale is rich in cyanobacteria, $\delta^{13}C_{kerogen}$ is generally more than −30‰, and both hydrocarbon-generating OM are planktonic algae. It is generally believed that planktonic algae have strong hydrocarbon generation capacity, while benthic algae rooted in soft silt have poor hydrocarbon generation capacity (Wang et al., 1994; Ye et al., 2012). However, the average $\delta^{13}C_{kerogen}$ of the $E_{2\text{-}3a}$ green algae is about 4‰ higher than that of the K_{1q} cyanobacteria, which is related to their carbon source utilization efficiency, photosynthetic intensity, and carbon sequestration process. The $\delta^{13}C_1$, $\delta^{13}C_2$, and $\delta^{13}C_3$ of the two types of shales tended to become heavier first and then lighter with increasing temperature (Fig. 11a, b, and c), which was mainly related to carbon isotope fractionation. The bond energy of $^{12}C-^{12}C$ is smaller than that of $^{13}C-^{13}C$. In the early stage of pyrolysis, hydrocarbon gases are mainly enriched in ^{12}C. When the lowest temperature of ^{13}C bond breaking is reached, ^{13}C is gradually enriched in hydrocarbon gases with increasing temperature (Fenton and Ritz, 1989), and kerogen further condensates to form carbon-rich residual material and eventually graphitization. This evolution of natural gas is controlled by the stage of hydrocarbon generation and evolution, but the influencing factors of carbon isotopes of non-hydrocarbon gases are complex, and the above trend is not obvious (Fig. 11d). This is consistent with the findings of Tang et al. (2000), Dieckmann et al. (2006), and Lewan and Roy (2012) et al.

However, it is interesting that, with the increase of simulation temperature, the carbon isotope of hydrocarbon gas in the shale rich in cyanobacteria and the shale rich in green algae evolves according to the above trend, and there seems to be a virtual line between them (Fig. 11a, b, and c), that is, the carbon isotope of the gas generated by green algae is always relatively heavy, while the carbon isotope of the gas generated by blue algae is always relatively light. This may be related to the obvious difference in $\delta^{13}C_{kerogen}$ between cyanobacteria and green algae. However, the fundamental reason is the difference in living habits between cyanobacteria and green algae. It is speculated that green algae mainly live in the surface and upper layers of water and their carbon source is mainly CO_2 in the atmosphere and HCO_3^- formed by its dissolution balance. However, cyanobacteria may live in the middle or even near the bottom of the water body, and their carbon sources include not only water-soluble CO_2 and HCO_3^- but also CO_2 and HCO_3^-, released by some plants, which may be one of the important reasons for the large difference in carbon isotopes of kerogen. In addition, there are obvious differences in the use of carbon sources, photosynthetic efficiency, and carbon sequestration efficiency between cyanobacteria and green algae, which finally lead to the respective characteristics of $\delta^{13}C_{kerogen}$, $\delta^{13}C_{extract}$, and the simulated evolution of $\delta^{13}C_{(HC\ gas)}$ (Maberly et al., 1992).

With the deepening of the thermal evolution of source rocks,

Table 7
Carbon isotopic composition of gases produced in water pyrolysis experiments.

Samples	Pyrolysis temperature	Stable carbon isotopic compositions, ‰, VPDB			
		C_1	C_2	C_3	CO_2
Aj1	280	−37.310	−27.208	−27.596	6.891
	300	−37.050	−26.982	−28.933	7.239
	330	−35.897	−26.584	−29.373	4.334
	340	−35.738	−30.387	−30.387	−30.202
	350	−36.688	−28.459	−32.076	2.831
	370	−34.617	−29.575	−33.981	3.963
	400	−39.603	−24.442	−34.093	1.886
	450	−38.362	−21.741	−30.617	1.153
	500	−39.368	−20.092	−30.694	1.461
Aj2	280	−36.302	−24.925	−27.193	0.526
	300	−35.738	−30.387	−30.387	−30.202
	330	−35.077	−25.083	−28.418	0.005
	340	−34.696	−25.435	−28.558	−0.029
	350	−36.485	−25.668	−29.144	0.039
	370	−36.422	−26.113	−30.938	−2.154
	400	−34.880	−24.014	−32.018	−3.258
	450	−32.524	−29.472	−29.472	−1.303
	500	−31.790	−23.411	−21.889	−3.456
Sc	315	−40.527	−33.782	−32.655	−3.977
	330	−39.210	−32.780	−31.711	−3.932
	340	−38.770	−32.670	−31.677	−3.085
	360	−40.052	−33.354	−32.245	−4.595
	370	−39.942	−33.727	−32.747	−3.851
	400	−42.537	−36.555	−34.456	−4.007
	450	−42.333	−35.033	−28.352	−5.473
	500	−39.169	−25.999	16.678	−7.360
Pc1	300	−37.604	−34.882	−34.019	0.949
	320	−41.921	−35.257	−35.704	0.569
	330	−40.964	−36.928	−36.004	0.321
	340	−42.622	−36.046	−36.061	2.073
	350	−41.289	−36.194	−35.724	1.777
	370	−42.626	−36.304	−36.600	1.818
	400	−45.008	−38.594	−36.946	0.750
	450	−44.164	−36.155	−32.653	−0.973
	500	−37.631	−24.494	/	0.149

Note: "/": not detected.

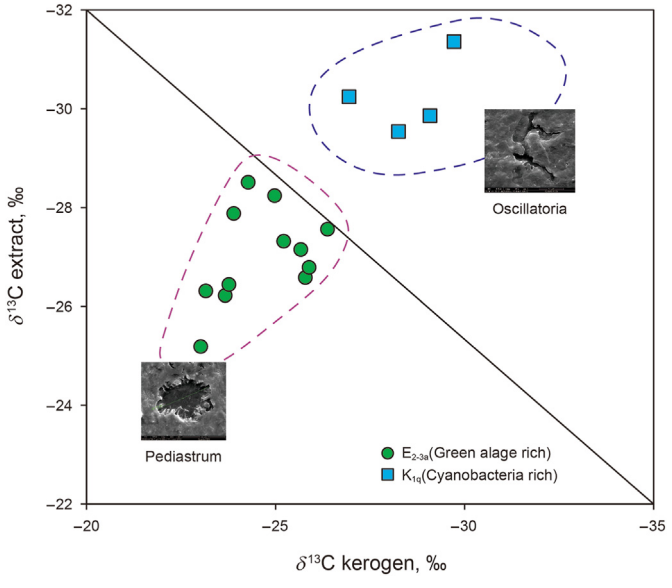

Fig. 10. Cross plots of carbon isotopes of kerogen and chloroform extracts from typical samples of the $E_{2\text{-}3a}$ and the K_{1q}.

Table 8
Carbon isotopic composition of typical samples of the $E_{2\text{-}3a}$ and the K_{1q}.

Formation	Samples	$\delta^{13}C_{extract}$, ‰	$\delta^{13}C_{kerogen}$, ‰	Algae
$E_{2\text{-}3a}$	AJ1	−27.15	−25.66	Green algae
	AJ2	−26.31	−23.15	
	AJ3	−26.22	−23.66	
	AJ4	−25.19	−23.01	
	AJ5	−26.44	−23.76	
	AJ6	−28.51	−24.27	
	AJ7	−27.56	−26.37	
	AJ8	−28.24	−24.97	
	DS1	−27.32	−25.21	
	DS2	−26.58	−25.78	
	DS3	−26.79	−25.88	
	DS4	−27.88	−23.89	
K_{1q}	SC	−29.54	−28.25	Cyanobacteria
	PC1	−30.24	−26.94	
	PC2	−29.86	−29.08	
	PC3	−31.36	−29.72	

the carbon isotopic composition also has a specific fractionation effect, but the $\delta^{13}C$ change of hydrocarbon OM in the same lifetime does not exceed 2‰–3‰ during the whole evolution process (Tissot, 1978), which was also verified in this study. The existing studies believe that the crude oil generated from these two sets of shale has no obvious difference in biomarkers and isoprenoid alkanes (Li et al., 2003), therefore, carbon isotope is one of the important methods to solve the problem of a mixed source of hydrocarbons generated from the K_{1q} and the $E_{2\text{-}3a}$ lacustrine shales in the Junggar Basin.

5. Conclusion

(1) Both shales of the $E_{2\text{-}3a}$ and the K_{1q} in the Junggar Basin have good oil generation ability. The main hydrocarbon-generating OM of the shales of the $E_{2\text{-}3a}$ is dominated by green algae (*Pediastrum*), while the main hydrocarbon-generating OM of the shales of the K_{1q} is dominated by cyanobacteria (*Oscillatoria*).

(2) Green algae and cyanobacteria have different hydrocarbon generation modes. Green algae have a low oil generation threshold, heavy oil quality, and no prominent oil peak, while cyanobacteria have the characteristics of late oil generation, concentrated hydrocarbon generation, and relatively light oil quality. This can also be well reflected in the composition of the crude oil group generated at different pyrolysis temperatures; that is, the closer the oil generation peak is, the higher the content of heavy components (resins and asphaltene), and the relative content of heavy components in the oil generated by green algae is always higher than that generated by cyanobacteria.

(3) Both green algae and cyanobacteria belong to planktic algae, but the carbon isotopes of green algae kerogen, extract, and pyrolysis hydrocarbon gas are significantly heavier than those of cyanobacteria, which may have obvious differences with their living habits, carbon source usage, photosynthetic efficiency, and carbon sequestration efficiency. Carbon isotope is one of the critical methods to solve the problem of mixed sources of hydrocarbons generated from the Meso-Cenozoic K_{1q} and $E_{2\text{-}3a}$ lacustrine shales in the Junggar Basin.

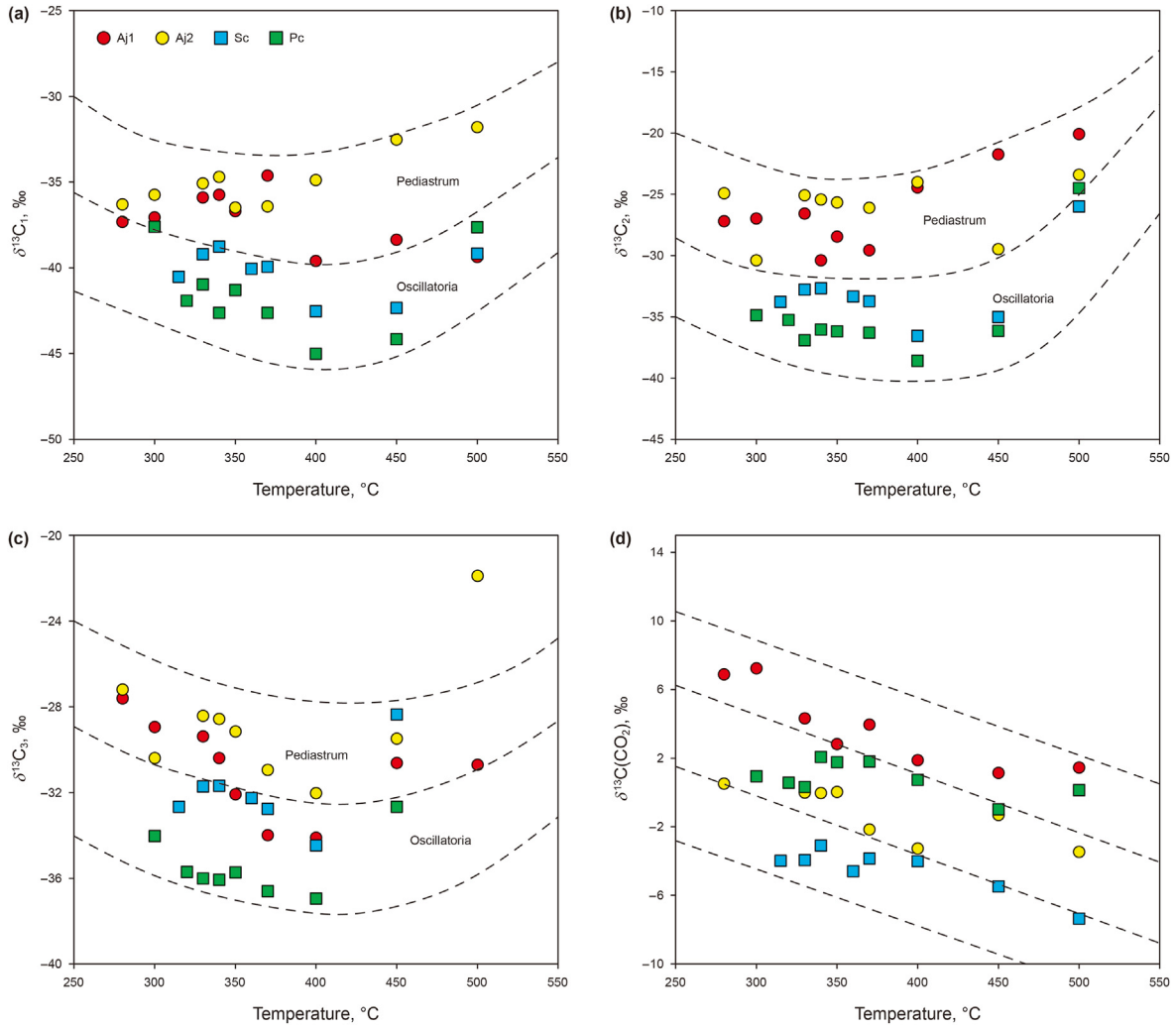

Fig. 11. Carbon isotope evolution of pyrolysis gases from typical samples of the $E_{2\text{-}3a}$ and the K_{1q}. Carbon isotope evolution diagram of methane from pyrolysis gas of the $E_{2\text{-}3a}$ samples rich in green algae and the K_{1q} samples rich in cyanobacteria (a); Carbon isotope evolution diagram of pyrolysis gas ethane for the $E_{2\text{-}3a}$ samples rich in green algae and the K_{1q} samples rich in cyanobacteria (b); Carbon isotope evolution diagram of pyrolytic gas propane in the $E_{2\text{-}3a}$ samples rich in green algae and the K_{1q} samples rich in cyanobacteria (c); Carbon isotope evolution diagram of pyrolytic gas CO_2 for the $E_{2\text{-}3a}$ samples rich in green algae and the K_{1q} samples rich in cyanobacteria (d).

Conflict of interest

We declare that we have no financial and personal relationships with other people or organizations that can inappropriately influence our work, there is no professional or other personal interest of any nature or kind in any product, service and/or company that could be construed as influencing the position presented in, or the review of, the manuscript entitled, "***Hydrocarbon generation differences of shales composed of green algal and cyanobacteria: A case study of Mesozoic and Cenozoic saline lacustrine shales in Junggar Basin, NW China***".

Acknowledgments

This work is financially supported by Xinjiang Oilfield Company of China (No. 2020-C4006). Thanks for the guidance and help of relevant experts from the Experimental Testing Research Institute of PetroChina Xinjiang Oilfield Branch, and thanks to the State Key Laboratory of Oil and Gas Resources and Exploration, China University of Petroleum (Beijing), for providing advanced experimental equipment, accurate experimental analysis results, and constructive guidance. Thanks to the editors and anonymous reviewers for their constructive comments, which greatly improved this article.

References

Brutemark, A., Lindehoff, E., Granéli, E., Granéli, W., 2009. Carbon isotope signature variability among cultured microalgae: influence of species, nutrients, and growth. J. Exp. Mar. Biol. Ecol. 372 (1–2), 98–105. https://doi.org/10.1016/j.jembe.2009.02.013.

Chen, J.P., Wang, X.L., Deng, C.P., Zhao, Z., Ni, Y.Y., Sun, Y.G., Yang, H.B., Wang, H.T., Liang, D.G., Zhu, R.K., Peng, X.L., 2015. Geochemical features of source rocks in the southern margin, Junggar Basin, Northwestern China. Acta Petrol. Sin. 36 (7), 767–780. https://doi.org/10.7623/syxb201507001 (in Chinese).

Chen, J.P., Deng, C.P., Wang, X.L., Ni, Y.Y., Sun, Y.G., Zhao, Z., Liao, J.D., Wang, P.R., Zhang, D.J., Liang, D.G., 2017. Formation mechanism of condensates, waxy and heavy oils in the southern margin of Junggar Basin. Sci. China Earth Sci. 47 (5), 567–585. https://doi.org/10.1007/s11430-016-9027-3 (in Chinese).

Chen, Y.Q., Wang, W.F., 2004. Structural evolution and pool-forming in Junggar Basin. Nat. Sci. J. China Univ. Pet. 3, 4-8+136 (in Chinese).

Collister, J., Ehrlich, R., Mango, F., Johnson, G., 2004. Modification of the petroleum system concept: origins of alkanes and isoprenoids in crude oils. AAPG (Am. Assoc. Pet. Geol.) Bull. 88, 587–611. https://doi.org/10.1306/01070403019.

Cook, A.C., Sherwood, N.R., 1991. Classification of oil shales, coals, and other organic-rich rocks. Org. Geochem. 17, 211–222. https://doi.org/10.1016/0146-

6380(91)90079-Y.
Dieckmann, V., Ondrak, R., Cramer, B., Horsfield, B., 2006. Deep basin gas: new insights from kinetic modeling and isotopic fractionation in deep-formed gas precursors. Mar. Petrol. Geol. 23 (2), 183–199. https://doi.org/10.1016/j.marpetgeo.2005.08.002.
Douglas, A.G., Sinninghe, D.J.S., Fowler, M.G., Eglinton, T.I., Leeuw, J.W., 1991. Unique distributions of hydrocarbons and sulfur compounds released by flash pyrolysis from the fossilized alga Gloeocapsomorpha Prisca, a major constituent in one of four Ordovician kerogens. Geochem. Cosmochim. Acta 55, 275–291. https://doi.org/10.1016/0016-7037(91)90417-4.
Du, J.H., Zhi, D.M., Li, J.Z., Yang, D.S., Tang, Y., Qi, X.F., Xiao, L.X., Wei, L.Y., 2019. A breakthrough of Well Gaotan 1 and exploration prospects of lower assemblage in the southern margin of Junggar Basin, NW China. Petrol. Explor. Dev. 46 (2), 205–215. https://doi.org/10.1016/S1876-3804(19)60003-0 (in Chinese).
Espitalie, J., Deroo, G., Marquis, F., 1985. La pyrolyse Rock-Eval et ses applications. Premiere partie. Rev. Inst. Fr. Pet. 40, 563–579. https://doi.org/10.2516/ogst:1986003.
Fenton, G.E., Ritz, D.A., 1989. Spatial variability of ^{13}C: ^{12}C and D: H inEcklonia radiata (C. Ag.) J. Agardh (Laminariales). Estuar. Coast Shelf Sci. 28 (1), 95–101. https://doi.org/10.1016/0272-7714(89)90044-9.
Foster, C.B., Wicander, R., Reed, J.D., 1990. Gloeocapsomorpha Prisca Zalessky., 1917. A new study part II: the origin of Kukersite, a new interpretation. Geobios-Lyon. 23, 133–140. https://doi.org/10.1016/S0016-6995(06)80045-8.
Gao, G., Liu, S.J., Jin, J., Zhang, Z.H., Liu, G.D., Xiang, B.L., Huang, Z.L., Kang, J.L., Gang, W.Z., 2023. A new discovery of physical property evolution of crude oil and insights into shale oil exploration. Acta Geochim 97 (5), 1561–1575. https://doi.org/10.19762/j.cnki.dizhixuebao.2023216.
Geel, V.B., 2001. Non - pollen palynomorphs. In: Smol, J.P., Birks, H.J.B., Last, W.M. (Eds.), Tracking Environmental Change Using Lake Sediments: Terrestrial, Algal, and Siliceous Indicators, vol. 3. Kluwer, Dordrecht, pp. 99–119. https://doi.org/10.1007/0-306-47668-1_6.
Hakimi, M.H., Hasiah, W.A., 2013. Organic geochemical characteristics and oil generating potential of the Upper Jurassic Safer shale sediments in the Marib-Shabowan basin. western Yemen. Org. Geochem. 54, 115–124. https://doi.org/10.1016/j.orggeochem.2012.10.003.
Han, Y.J., Mahlstedt, N., Horsfield, B., 2015. The Barnett Shale: compositional fractionation associated with intraformational petroleum migration, retention, and expulsion. AAPG (Am. Assoc. Pet. Geol.) Bull. https://doi.org/10.1306/06231514113.
Hutton, A.C., Kantsler, A.J., Cook, A.C., McKirdy, D.M., 1980. Organic matter in oil shales. Aust. Pet. Explor. Assoc. J. 20, 44–68. https://doi.org/10.1071/AJ79005.
Hutton, A.C., 1987. Petrographic approach to beneficiation of Australian oil shales. Fuel 66, 314–318. https://doi.org/10.1016/0016-2361(87)90085-8.
Jankovská, V., Komárek, J., 2000. Indicative value of Pediastrum and other coccal green algae in palaeoecology. Folia Geobot. 35, 59–82. https://doi.org/10.1007/BF02803087.
Jin, X.F., 2000. Comparative experimental study on hydrocarbon generation yields of palynology and algae. Petrol. Explor. Dev. 3, 28-32+111-120 (in Chinese).
Jones, T.D., Ridgwell, A., Lunt, D.J., Maslin, M.A., Schmidt, D.N., Valdes, P.J., 2010. Palaeogene perspective on climate sensitivity and methane hydrate instability. Phil. Trans.: Math. Phys. Eng. Sci. 368 (1919), 2395–2415. https://doi.org/10.1098/rsta.2010.0053.
Klemme, H.D., Ulmishek, G.F., 1991. Effective petroleum source rocks of the world; stratigraphic distribution and controlling depositional factors. AAPG (Am. Assoc. Pet. Geol.) Bull. https://doi.org/10.1306/0C9B2A47-1710-11D7-8645000102C1865D.
Klewiah, I., Berawala, D.S., Walker, H.C., Andersen, P.Ø., Nadeau, P.H., 2019. Review of experimental sorption studies of co 2 and ch 4 in shales. J. Nat. Gas Sci. Eng. 73. https://doi.org/10.1016/j.jngse.2019.103045.
Komárek, J., Jankovská, V., 2001. Review of the green algal genus Pediastrum: implication for pollen analytical research. Germany: Bibl. Phycol. 1–111. https://doi.org/10.1641/B580206.
Lafargue, E., Marquis, F., Pillot, D., 1998. Rock-Eval 6 applications in hydrocarbon exploration, production, and soil contamination studies. Oil Gas Sci. Technol. Rev. IFP 53, 421–437. https://doi.org/10.2516/OGST:1998036.
Laws, E.A., Popp, B.N., Bidigare, R.R., Kennicutt, M.C., Macko, S.A., 1995. Dependence of phytoplankton carbon isotopic composition on growth rate and [CO_2] aq: theoretical considerations and experimental results. Geochem. Cosmochim. Acta 59 (6), 1131–1138. https://doi.org/10.1016/0016-7037(95)00030-4.
Lewan, M.D., Winters, J.C., Mcdonald, J.H., 1979. Generation of oil-like pyrolyzates from organic-rich shales. Science 203 (4383), 897–899. https://doi.org/10.1126/science.203.4383.897.
Lewan, M.D., 1983. Effects of thermal maturation on stable organic carbon isotopes as determined by hydrous pyrolysis. Geochem. Cosmochim. Acta 47, 1471–1479. https://doi.org/10.1016/0016-7037(83)90306-X.
Lewan, M.D., Kotarba, M.J., Więcław, D., Piestrzyński, A., 2008. Evaluating transition metal catalysis in gas generation from the Permian. Geochem. Cosmochim. Acta 72 (16), 4069–4093. https://doi.org/10.1016/j.gca.2008.06.003.
Lewan, M.D., Roy, S., 2012. Role of water in hydrocarbon generation from type-i kerogen in mahogany oil shale of the green river formation. Org. Geochem. 42 (1), 31–41. https://doi.org/10.1016/j.orggeochem.2010.10.004.
Li, X.Y., Shao, Y., Li, T.M., 2003. Three oil-reservoir combinations in the south marginal of Jungar Basin, Northwest China. Petrol. Explor. Dev. 6, 32–34. https://doi.org/10.1007/BF02974893 (in Chinese).
Lin, J.W., Xie, X.M., Wen, Z.G., Wu, F.T., Xu, J., Ma, Z.L., Zhang, L., 2022. A comparative study on the geochemical characteristics of expelled and retained oil from hydrocarbon generation simulation of Australian Tasmanian oil shaley I: fraction and isotopic compositions. Pet. Geol. Exp. 44 (1), 150–159 (in Chinese).
Loucks, R.G., Reed, R.M., Ruppel, S.C., Jarvie, D.M., 2009. Morphology, genesis, and distribution of nanometer-scale pores in siliceous mudstones of the Mississippian Barnett shale. J. Sediment. Res. 79 (11–12), 848–861. https://doi.org/10.2110/jsr.2009.092.
Maberly, S.C., Raven, J.A., Johnston, A.M., 1992. Discrimination between ^{12}C and ^{13}C by marine plants. Oecologia 91 (4), 481–492. https://doi.org/10.1007/BF00650320.
Mukhopadhyay, P.K., Wade, J.A., Kruge, M.A., 1995. Organic facies and maturation of Cretaceous/Jurassic rocks and possible oil-source rock correlation based on pyrolysis of asphaltenes, Scotian basin, Canada. Org. Geochem. 22, 85–104. https://doi.org/10.1016/0146-6380(95)90010-1.
Peters, K.E., 1986. Guidelines for evaluating petroleum source using programmed pyrolysis. Am. Assoc. Petrol. Geol. Bull. 70, 318–329. https://doi.org/10.1306/94885688-1704-11D7-8645000102C1865D.
Peters, K.E., Walters, C.C., Mankiewicz, P.J., 2006. Evaluation of kinetic uncertainty in numerical models of petroleum generation. AAPG (Am. Assoc. Pet. Geol.) Bull. 90 (3), 387–403. https://doi.org/10.1306/10140505122.
Picard, M.D., 1985. The hypothesis of oil shale genesis, Green River Formation, northeast Utah, northwest Colorado, and southwest Wyoming. In: Picard, M.D. (Ed.), Geology and Energy Resources. Uinta Basin of Utah. Utah Geological Association, pp. 92–96.
Primio, D.R., Horsfield, B., Guzman-Vega, M.A., 2000. Determining the temperature of petroleum formation from the kinetic properties of petroleum asphaltenes. Nature 406, 173–176. https://doi.org/10.1038/35018046.
Pu, X., Liu, S., Hao, S., 1998. The biomarkers' characteristics and significance of saturated hydrocarbon derived from Gloeocapsomorpha Prisca laboratory simulation by hydrous pyrolysis. Bull. China Soc. Mineral Petrol. Geochem. 17, 102–106 (in Chinese).
Quigley, T.M., Mackenzie, A.S., 1988. The temperature of oil and gas formation in the sub-surface. Nature 333 (6173), 549–552. https://doi.org/10.1038/333549a0.
Ritter, U., 2003. Solubility of petroleum compounds in kerogen: implications for petroleum expulsion. Org. Geochem. 34 (3), 319–326. https://doi.org/10.1016/S0146-6380(02)00245-0.
Robinson, W.E., 1969. Kerogen of the Green River formation. In: Eglinton, G., Murphy, M.T.J. (Eds.), Org. Geochem. Springer, Berlin\Heidelberg\New York, pp. 619–637. https://doi.org/10.1007/978-3-642-87734-6_33.
Ruble, T.E., Lewan, M.D., Philp, R.Paul, 2003. New insights on the Green River petroleum system in the Uinta basin from hydrous-pyrolysis experiments: reply. AAPG (Am. Assoc. Pet. Geol.) Bull. 87 (9), 1535–1541. https://doi.org/10.1306/0423030137r.
Rullkotter, J., Leythaeuser, D., Horsfield, B., Littke, R., Mann, U., Muller, P.J., Radke, M., Schaefer, R.G., Schenk, H.J., Schwochau, K., Witte, E.G., Welte, D.H., 1987. Organic matter maturation under the influence of a deep intrusive heat source: a natural experiment for quantitation of hydrocarbon generation and expulsion from a petroleum source rock (Toarcian Shale, northern Germany). In: Mattavelli, L., Novelli, L. (Eds.), Advances in Organic Geochemistry, vol. 13. Org. Geochem, pp. 847–856. https://doi.org/10.1016/0146-6380(88)90237-9.
Sandvik, E.I., Young, W.A., Curry, D.J., 1992. Expulsion from hydrocarbon sources: the role of organic absorption. Org. Geochem. 19 (1–3), 77–87. https://doi.org/10.1016/0146-6380(92)90028-V.
Saxby, J.D., 1980. Organic geochemistry of oil shales. In: Cook, A.C., Kantsler, A.J. (Eds.), Oil Shale Petrology Workshop. Wollongong, Australia, pp. 63–69. https://doi.org/10.1016/0146-6380(90)90092-E.
Schenk, H.J., di Primio, R., Horsfield, B., 1997. The conversion of oil into gas in petroleum reservoirs. Part I. Comparative kinetic investigation of gas generation from crude oils of lacustrine, marine, and fluviodeltaic origin by programmed-temperature closed-system pyrolysis. Org. Geochem. 26, 467–481. https://doi.org/10.1016/S0146-6380(97)00024-7.
Schidlowski, M., Golubic, S., Kimberley, M.M., McKirdy, D.M., Trudinger, P.A. (Eds.), 1992. Early Organic Evolution: Implications for Mineral and Energy Resources. Springer-Verlag, New York. https://doi.org/10.1016/0016-7037(93)90427-X.
Shang, L., Liu, X., Bian, B.L., 2011. Sedimentary facies in the Triassic Karamay formation, Beisantai, Junggar Basin, Xinjiang. Sediment. Geol. Tethyan Geol. 31 (3), 33–38. https://doi.org/10.1016/S1002-0160(11)60127-6 (in Chinese).
Sharkey, T.D., Berry, J.A., 1986. Carbon isotope fractionation of algae is influenced by an inducible CO_2 concentrating mechanism. In: Lucas, W.J., Berry, J.A. (Eds.), Inorganic Carbon Uptake by Aquatic Photosynthetic Organisms. American Society of Plant Physiologists, Rockville, pp. 389–401.
Smith, W.D., St Peter, C.J., Naylor, R.D., Mukhopadhyay, P.K., Kalkreuth, W.D., Ball, F.D., Macauley, G., 1991. Composition and depositional environment of major eastern Canadian oil shales. Int. J. Coal Geol. 19, 385–438. https://doi.org/10.1016/0166-5162(91)90028-H.
Stach, E., Mackowsky, M-Th, Teichmüller, M., Taylor, G.F., Chandra, G., Teichmüller, R., 1982. Stach's Textbook of Coal Petrology, second ed. Gebrüder Borntraeger, Berlin. https://doi.org/10.1016/0016-2361(76)90104-6.
Stahl, W.J., 1974. Carbon isotope fractionation in natural gases. Nature 251, 134–135. https://doi.org/10.1038/251134a0.
Tang, Y., Perry, J.K., Jensen, P.D., Schoell, M., 2000. Mathematical modeling of stable carbon isotope ratios in natural gases. Geochem. Cosmochim. Acta 15, 64. https://doi.org/10.1016/s0016-7037(00)00377-x.
Taylor, G.H., Teichmüller, M., Davis, A., Diessel, C.F.K., Littke, R., Robert, P., 1998. Organic Petrology. Gebrüder Borntraeger, Berlin. https://doi.org/10.1016/S1342-

937X(05)70115-5.
Tian, A.Q., Chen, S., Yu, Y.X., Xiu, J.L., Jin, F., 2022. Layered deformation characteristics, the formation mechanism of strike-slip faults on the western edge of Mosuowan uplift. Geosciences 1–15 (in Chinese).
Tissot, B.P., 1978. Petroleum formation and occurrence. J. Sediment. Res. 55. https://doi.org/10.1016/0012-8252(80)90071-9.
Tissot, B.P., Pelet, R., Ungerer, P.H., 1987. Thermal history of sedimentary basins, maturation indices, and kinetics of oil and gas generation. Am. Assoc. Petrol. Geol. Bull. 71 (12), 1445–1466. https://doi.org/10.1306/703C80E7-1707-11D7-8645000102C1865D.
Ungger, P., Pelet, R., 1987. Extrapolation of the kinetics of oil and gas formation from laboratory experiments to sedimentary. Nature 327, 52–54. https://doi.org/10.1038/327052a0.
Wang, K.F., Zhang, Y.L., Wu, G.X., Li, Y.Y., He, C.Q., Zhang, H.Z., 1994. Study on the thermal simulation of oil generation from Pediastrum. J. Tongji Univ. Nat. Sci. (2), 184–191 (in Chinese).
Wang, B., Wu, M., Wang, X.L., Zhang, Y.Q., Cao, J., 2011. Source rock features and evaluation of Triassic strata in the central Junggar Basin. J. Southwest Pet. Univ., Sci. Technol. Ed. 33 (2). https://doi.org/10.3863/j.issn.1674-5086.2011.02.002, 12-20+7-8 (in Chinese).
Wang, X.J., Song, Y., Zheng, M.L., Ren, H.J., Wu, H.S., He, W.J., Wang, T., Wang, X.T., Zhao, C.Y., Guo, J.C., 2021. Composite petroleum system and multi-stage hydrocarbon accumulation in Junggar Basin. China Pet. Explor. 26 (4), 29–43. https://doi.org/10.3969/j.issn.1672-7703.2021.04.003 (in Chinese).
Weckström, K., Weckström, J., Yliniemi, L.M., 2010. The ecology of Pediastrum (Chlorophyceae) in subarctic lakes and their potential as paleobioindicators. J. Paleolimnol. 43 (1), 61–73. https://doi.org/10.1007/s10933-009-9314-y.
Yang, H.B., Chen, L., Kong, Y.H., 2004. A novel classification of structural units in Junggar Basin. Xinjiang Pet. Geol. (6), 686–688. https://doi.org/10.3969/j.issn.1001-3873.2004.06.034 (in Chinese).
Ye, Y., Liu, W.H., Tenggeer, Wang, J., Ma, L.B., Li, Y.C., 2012. Research on cyanobacteria from the chaohu lake during a simulating process of decaying: changes in morphology and organic composition. Acta Micropalaeontol. Sin. 29 (2), 152–160. https://doi.org/10.1007/s11783-011-0280-z (in Chinese).
Yu, M., Gao, G., Jin, J., Ma, W.Y., He, D., Xiang, B.L., Fan, K.T., Liu, M., 2022. Hydrocarbon generation simulation of coaly source rocks in the Lower combination on the southern margin of Junggar Basin and indications for oil and gas sources of well Gaotan 1. Pet. Geol. Exp. 44 (4), 687–697 (in Chinese).
Zamaloa, M., Tell, G., 2005. The fossil record of freshwater micro-algae Pediastrum meyen (Chlorophyceae) in Southern South America. J. Paleolimnol. 34 (4), 433–444. https://doi.org/10.1007/s10933-005-5804-8.